CHARACTERIZING SPECTRAL DIVERSITY IN CARBONACEOUS CHONDRITES AND LINKING TO ASTEROIDS WITH MICROIMAGING SPECTROSCOPY. S. A. Parra[1], B. L. Ehlmann[1,2], R. N. Greenberger[1], Z. Small[2], P. Mouroulis[2], M. Velbel[3,4] [1]Div. of Geological & Planetary Sciences, California Institute of Technology, Pasadena, CA (sparra@caltech.edu), [2]Jet Propulsion Laboratory, California Institute of Technology, Pasadena, CA. [3]Michigan State University, Lansing, MI. [4]Smithsonian Institution, Washington, DC.

Introduction: Primitive asteroids have undergone relatively little melting and differentiation, record alteration processes in the early Solar System, and may shed light on the delivery of volatiles and organics to terrestrial planets [1, 2]. Telescopic visible and shortwave infrared (VSWIR) spectroscopy of primitive asteroids has enabled the identification of broad spectral classes, and thus compositions, indicative of certain alteration processes [1, 3, 4]. However, these mostly spatially unresolved telescopic observations preclude spectral mapping to isolate endmembers. This inhibits tying the specific, observed spectral feature differences to particular phases, alteration histories, and petrologic contexts.

Microimaging VSWIR spectroscopy of carbonaceous chondrites, which are meteorites that originate from primitive asteroids, provides μm-scale records of formation and alteration processes undergone by the parent bodies [2, 5]. VSWIR microimaging spectroscopy enables rapid and non-destructive spectral mapping of samples at the 10's to 100's of microns-scale [6], improving upon previous bulk powder VSWIR characterizations of carbonaceous chondrites by preserving the chondrites' petrologic textures and heterogeneity in spectral properties. Spectral mapping enables a more precise identification of the compositional drivers behind the spectral features observed, thereby minimizing occlusion by spectrally opaque phases [4, 7]. As such, the motivations for this work are to characterize the heterogeneities and distributions of observed spectral diversity in a suite of carbonaceous chondrites, and ultimately to link these to the spectral diversity observed in primitive asteroids.

Methods: We collected spectral image cubes for each chondrite with the Ultra-Compact Imaging Spectrometer (UCIS) at the Jet Propulsion Laboratory (JPL). UCIS is an imaging spectrometer capable of observing the 0.4 – 2.6μm wavelength range at a ~80μm/pixel spatial resolution [8]. Data were measured with 20 ms integration times and spectra were corrected to reflectance by dividing by a 20% Spectralon reflectance target and multiplying by its known spectral properties. We measured samples from 24 carbonaceous chondrites over a range in the degree of aqueous alteration and thermal metamorphism experienced. A subset of measured chondrites with varying chondrule versus alteration phase-rich matrix fraction are described here (Table 1).

As a first pass examination of observable spectral diversity, we prepared parameter maps from the image cubes to map characteristic absorptions for certain compositions [6], leading to a quick visualization of compositional heterogeneities.

Sample Name	Type	Provider
SCO 06043	CM1	NASA JSC
Murray	CM2	Caltech
NWA 7502	CR2	Caltech
Leoville	CV3	Caltech
Tagish Lake	C2, ungrouped	University of Alberta

Table 1. A subset of the carbonaceous chondrites included in this study for VSWIR microimaging spectroscopy.

We also performed principal component analysis (PCA) to identify key axes of dataset variance [9, 10, 11]. This enables a more direct identification of single or co-varying spectral endmembers that drive the observed diversity in the carbonaceous chondrites.

To apply this technique, the constituent spectra in each sample-specific image cube were pre-processed using a similar pipeline to that developed by [11] for the expanded Bus taxonomy of asteroids. Each spectrum was resampled to minimize noise through a cubic spline fitting procedure prior to a de-sloping step by dividing the resampled spectrum by a linear least squares slope fit. Removing the slope was observed by [11] to increase sensitivity to other features. The spectra were then normalized and mean subtracted at each channel to yield residuals for a more sensitive PCA analysis. To then compute the values of each meteorite spectrum for each principal component, the transpose of the eigenvector was multiplied by the transpose of the mean-subtracted reflectances, as shown in Eq. (1) below:

$$PC_x = [E_x^T][D^T] \quad (1)$$

where PC_x is principal component x and E_x is eigenvector x, taken from the eigenvector set evaluated with the entire chondrite data set encompassing all image cubes. D is the column vector containing an individual reflectance spectrum, normalized to unity at 0.55μm, from which the mean reflectance value has been subtracted at each wavelength.

Parameter Map Observations: The subset of chondrites listed were mapped according to the characteristic absorptions for Fe-Mg phyllosilicates (2.3-μm absorption), olivine (1-μm broad absorption), and H_2O

(1.9-μm band depth) to show the spatial distribution of aqueous alteration and fraction of chondrules (Fig. 1).

with spectra having a deeper 1μm band suggestive of greater olivine content (Fig. 2).

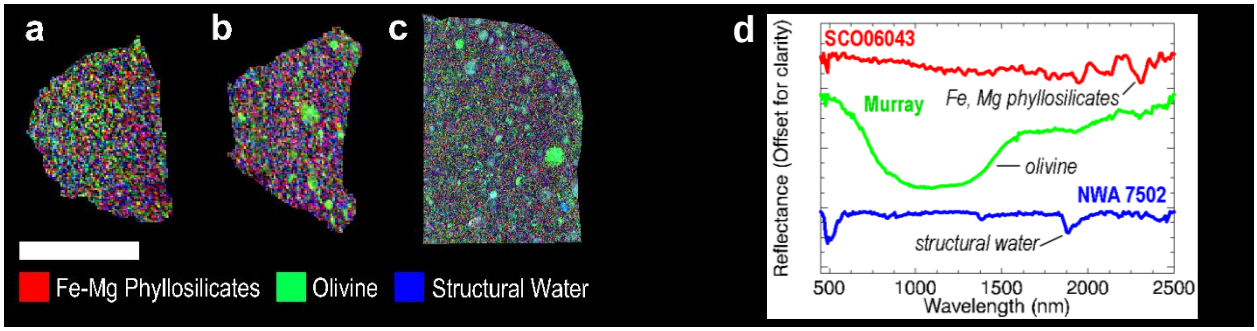

Figure 1. Example of the heterogeneous textures across (a) CM1 chondrite SCO06043, (b) CM2 chondrite Murray, and (c) subsample of CR2 chondrite NWA7502. Representative spectra for each parameter are shown in (d).Scale bar is 1cm for (a), (b); 2cm for (c).

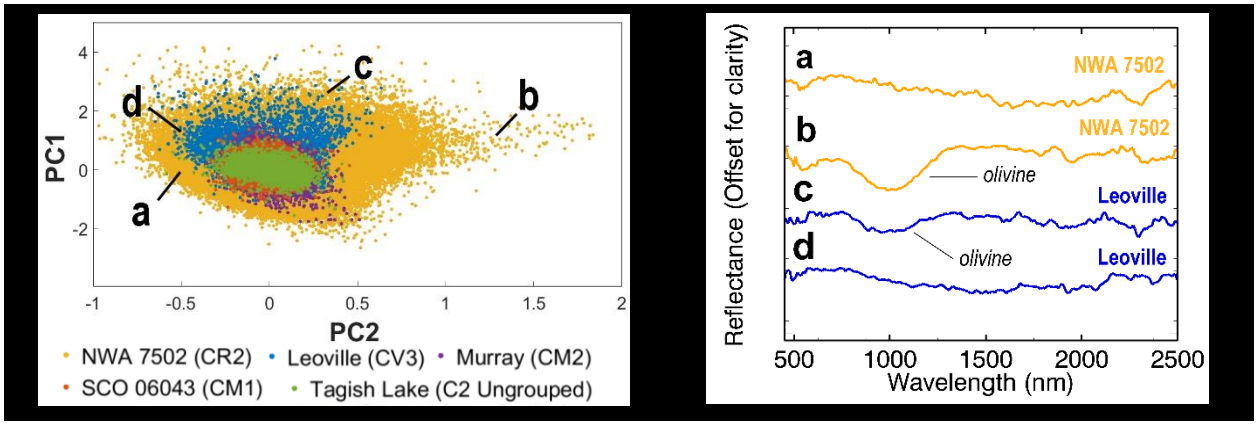

Figure 2. (left) Results for PC2 vs PC1.; (right) Spectra for NWA 7502 and Leoville chondrites, supporting the trend observed in the PC plot with regards to olivine content, indicated by a variable 1μm band depth.

The most readily apparent difference in the meteorite parameter maps is the abundance of olivine and pyroxene-rich chondrules. In the chondrite samples with no observable chondrules, however, olivine and pyroxene still occur as finer regions distributed heterogeneously the aqueously altered matrix (Fig. 1a). Chondrule abundance is thus variable, even within chondrite groups (e.g., CM chondrites in Fig. 1a vs 1b).

Principal Component Analysis: The first principal component (PC1) contained 70.9% of the variance in the data set, whereas PC2 only captured 7.8% of the variance. The top 16 PCs were necessary to achieve 95% of the variance, and the top 31 PCs to achieve 99% .

Plotting the spectra for each image cube in PC1 and PC2 (Fig. 2), we observed a roughly equant data cloud, with differing behaviors observed in the CR2/CV3 chondrite image cubes. The magnitude and distribution of all the plotted PCs are similar to the trend seen by [11] in asteroids for the first two principal components. This suggests comparable spectral diversities, which in [11] arose primarily from differences in band depths at 1 and 2 μm, suggesting variable olivine and pyroxene content. Indeed, the CR2/CV3 chondrites display lobes

Future Work: Further analysis will characterize inter- and intra- carbonaceous chondrite variability, as was observed by spectral parameter mapping, to further elucidate the drivers of spectral variability. Using the eigenvector set published by [11] for the expanded Bus taxonomy of asteroids, we will also directly compare the spectral diversity of the chondrite samples to that of primitive asteroids as a way to connect chondrites to their parent asteroids and associated alteration histories.

Acknowledgments: This work was funded by a NASA Emerging Worlds grant to B.L.E. (#80NSSC18K0593). A portion of this work was carried out at the Jet Propulsion Laboratory, California Institute of Technology. Spectral processing procedures were tested with spectral data supplied by Francesca DeMeo, EAPS, MIT.

References: [1] DeMeo, F. E., & Carry, B. (2014) *Nature*, 505(7485), 629–634. [2] Johansen, A., et al., (2015) *Science Advances, 1*(3), e1500109. [3] Burbine, T. H., & Binzel, R. P. (2002) *Icarus*, *159*(2), 468–499. [4] Takir, D., & Emery, J. P. (2012) *Icarus*, *219*(2), 641–654. [5] Scott, E. R. (2007) *Ann. Rev. of Earth & Plan. Sci.*, *35*(1), 577–620. [6] Greenberger, R. N., et al., (2015) *GSA Today*, *25*(12), 4–10. [7] Takir, D., et al. (2013) *Meteor. & Plan. Sci.*, *48*(9), 1618–1637. [8] Van Gorp, B., et al., (2014) *Journal of App. Rem. Sens.*, *8*(1), 084988. [9] Smith, M. O., et al., (1985) *JGR: Solid Earth*, *90*(S02), C797–C804. [10] Plaza, A., et al., (2009) *Remote Sens. of Env.*, *113*, S110–S122. [11] DeMeo, et al., (2009) *Icarus*, *202*(1), 160–180.